

On off-grid green solar panel supplied edge computing

Roberto Beraldi, Gabriele Proietti Mattia
University of Rome "La Sapienza"
Rome, Italy

Abstract—We consider the case of a group of communicating edge nodes only supplied with photovoltaic (PV) panels. This configuration makes the deploy green if all the data is elaborated locally, but a minimal (if nothing) communication with a remote server. This model has several characteristics. Since the amount of storable energy is limited by the battery capacity, the solar energy at an edge node with fully charged battery cannot be further accumulated, which is an indirect source of inefficiency. On the other hand, the energy consumed by edge nodes is tied to the activity of the nodes. Roughly an edge node in an idle state consumes less than one third of the power consumed when elaborating data, while the energy cost to move data among the edge nodes is usually less than the one required to elaborate them (which is the case in many applications). As a consequence an edge node which is running out of green energy can conveniently offload its computations to energy richer nodes in idle states. This paper reports some preliminary results of this form of green cooperation.

I. INTRODUCTION

The amount of data generated by IoT devices is expected to increase exponentially over the next years [1]. Edge computing may alleviate the need to transfer data to a cloud server by performing data elaboration closer to the data sources [2]. With the improvement in their performances, complex elaborations are also possible at the edge. For example, accelerator-based single-board computers (SBCs) showing high performance are being used as edge devices to run the inferencing part of the artificial intelligence (AI) model to deploy intelligent applications[3]. Besides being valuable for performance reasons, local elaboration is also a first step towards a reduction of pollution. Moving data to remote servers has in fact a no zero carbon footprint due to all the telecommunication equipments involved into data transmission and of course to use of the data centres [4].

In the idle state the energy consumed by an edge device is one third or less of the power needed when executing code. For example, [3] reported that the NVIDIA Jetson Xavier NX consumes 15.2 W when running YOLOv3 image detectors, and only 3.6 W when idle. Another element to add to the picture is the cost reduction of the Wh [Watt per hour] of batteries and the increasing efficiency of photovoltaics (PV) panels, that makes it possible to design green edge computing systems, that are energy self-sustainable (To ensure service continuity this deploy can go side-by-side with classic grid powered architectures). We here focus on a use-case scenario where a set of off-grid PV supplied edge nodes with their own camera all implement a common service of image detection,

so that a node can delegate the inspection of an image acquired by its own camera, to another node in the set (task offloading). This can be a scenario of traffic monitoring in a smart city.

A. Concept and motivation

The distributed nature of edge/fog resources makes it harder to exploit locally-produced green energy as more sites are considered [5].

In general, the amount of solar radiation converted by a PV panel into electrical energy depends, besides exogenous variables, e.g. weather conditions, on the orientation of the panels, and the specific day of the year. It is reasonable to assume that due to mechanical or other constrains, the orientation of panels in this set is different, so that nodes other things being equal have different green energy production. In addition, the state of these nodes (idle or working) may also differ.

Since the amount of storable energy is limited by the battery capacity, the solar energy at an edge node with fully charged battery cannot be further accumulated, which is an indirect source of inefficiency. We call this not accumulated energy, *energy surplus* loss. In order to consume as much green energy as possible it is worth for an edge node that is running out of green energy to offload image detection tasks to nodes with (almost) full battery at risk of energy surplus loss. This offload is globally energy efficient since the energy consumed to move (send) the image data from one node to another is usually less than to making computation on it.

The contribution of this paper is (i) a characterisation an off-grid green edge computing model and (ii) an initial evaluation of the benefit of task green energy aware task offloading.

The paper is organised as following. Section II reports the related work, Section III introduces the background concept; in Section IV the dependency of orientation and day of the year on the energy production is analysed, and a baseline evaluation of a PV supplied edge station is given in Section V. The proposed seeker-giver protocol is presented in Section VI and conclusion in Section VII. For completeness some algebraic notion are reported in the Appendix.

II. RELATED WORK

Several papers address the problem of energy efficiency in fog computing, via load balancing or proper resource allocation. [6] proposes an energy-aware load balancing and scheduling (ELBS) method based on fog computing. The work

reports an energy consumption model of the workload on the fog node. [7] designs a novel Energy-aware Data Offloading (EaDO) technique to minimize the energy consumption and latency in the industrial environment. [8] studied a sustainable infrastructure in Fog-Cloud environment for processing delay-intensive and resource-intensive applications with an optimal task offloading strategy. The proposed offloading strategy optimizes two Quality-of-Service (QoS) parameters such as energy consumption and computational time. The model in these papers include a cloud layer where the computation is eventually performed. [5] presented an energy-efficient Fog architecture considering the integration of renewable energy. Three resource allocation algorithms and three consolidation policies were studied.

III. BACKGROUND: SOLAR GEOMETRY

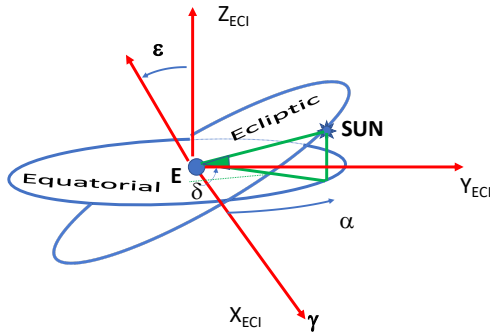


Figure 1: The position of the sun in the sky is identified through two angles: the Right Ascension (α) and the declination (δ). The movement of the sun is due to the earth rotation and revolution.

The apparent movement of the sun in the sky is due to two rotations: the earth's rotation around the earth's axis with a period of one sidereal day, and the earth's revolution around the center of gravity of the earth-sun system with a period of one sidereal year. The two rotations take place on two planes respectively called equatorial and ecliptic plane, which are inclined by $\epsilon = 23.4^\circ$. The intersection of the planes defines a line called the equinox line. To describe the motion it is convenient to use a geocentric coordinate system (see Figure 1). We use a simple model to derive the position of the sun \mathbf{d} , in which the orbit around the sun is circular and the speed of the earth is constant. The position depends not only on the time but also on the geographic latitude of the earth and on the day of the year. The motion is first described in the so-called ECI frame and then transformed into the horizontal frame, which is used to orient solar panels.

The Earth-Centred-Inertial (ECI) frame has origin at the center of mass of the earth, the X axis on the equinox line pointing towards the vernal equinox (denoted as point γ , Z

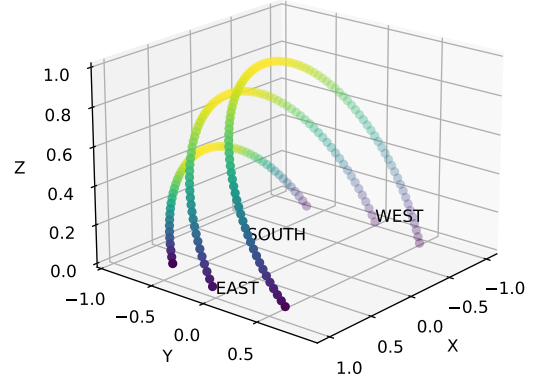


Figure 2: Example of sun path in the NEU frame at the equinox, winter and summer solstice, latitude 42° derived from Equation 1. At the equinox, the sun rises due east and sets due west. The duration of the day is longest at summer solstice and shortest at the winter solstice.

on the the (mean) earth's rotation axis, $Y = Z \times X^1$. the Earth-Centred-Earth Fixed (ECEF) frame that co-rotates with the earth. The ECEF and ECI frames are overlapped every sidereal day. The X and Y axis points towards longitude 0° (Greenwich meridian) and $e 90^\circ$ (east).

The position of the sun in the ECI frame can be expressed in Cartesian coordinates with following unit length vector:

$$\mathbf{d}_{ECI} = \begin{bmatrix} x_S \\ y_S \\ z_S \end{bmatrix} = \begin{bmatrix} \cos\delta\cos\alpha \\ \cos\delta\sin\alpha \\ \sin\delta \end{bmatrix}$$

from which:

$$\alpha = \text{tg}^{-1}\left(\frac{y_S}{x_S}\right)$$

$$\delta = \text{sin}^{-1}z_S$$

where α and δ are two angles: the Right Ascension (RA) which is the angle from the vernal equinox measured along the equator and the declination the angle with the equatorial plane, see Figure 1.

By definition, at vernal equinox (21 March), $d_{ECI}=(1,0,0)$ so that $\alpha = 0$ and $\delta = 0$. A simple relationship between α and δ is the following. As the ecliptic plane is tilted of ϵ , its normal in the ECI plane is $\mathbf{n} = (0, -\text{sin}\epsilon, \text{cos}\epsilon)$. The points on the vertical line (parallel to Z_{ECI}) passing from the sun with given α and δ , have coordinates $\mathbf{p} = (\text{cos}\alpha, \text{sin}\alpha, \text{tg}\delta)$. Hence, the intersection with the ecliptic plane is the point $\mathbf{p} \cdot \mathbf{n} = 0$, so that the relationship between α and δ is:

$$\delta = \text{tg}^{-1}(\text{tg}\epsilon \times \text{sin}\alpha) \approx \epsilon \times \text{sin}\alpha$$

¹Due to slightly changes of the earth's axis rotation over time, it is common to adopt for the definition the orientation of the axis at a given date. This sync point is called an epoch. ECI J2000 refers to the orientation at the 12:00 Terrestrial Time on 1 January 2000.

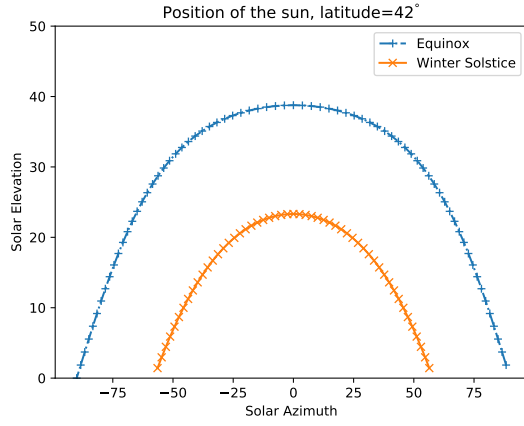


Figure 3: Example of solar diagram for the winter solstice and equinox.

which the relationship in [9]. Days are numbered from January first and during day N the α is fixed:

$$\alpha(N) = \frac{360}{365}(N + \Delta\gamma)$$

where $\Delta\gamma$ is the number of days from the last vernal equinox (Mach 20) from December 31, $\Delta\gamma = 286$. The value α is the right ascension of the sun during day N , which corresponds to the sun on the local meridian of the observer.

The NEU frame has the origin on the surface of the earth, the Z that points up to the sky towards the zenith (opposite to the plumb line), Y points towards the true North and X points towards East. The XY axis is tangent to the earth (assumed sphere). For this reason the frame is also called the horizontal frame and it is used to define the orientation of the panel on the earth.

The position of the sun \mathbf{d} in the NEU frame is found through the following linear mapping:

$$\mathbf{d} = \begin{pmatrix} x \\ y \\ z \end{pmatrix} = \begin{pmatrix} c_{\beta_z} & -s_{\beta_z} & 0 \\ c_{\beta_x}s_{\beta_z} & c_{\beta_x}c_{\beta_z} & -s_{\beta_x} \\ s_{\beta_x}s_{\beta_z} & c_{\beta_x}s_{\beta_x} & c_{\beta_x} \end{pmatrix} \begin{pmatrix} \cos\delta\cos\alpha \\ \cos\delta\sin\alpha \\ \sin\delta \end{pmatrix} \quad (1)$$

where $c_{\beta} = \cos\beta$ and $s_{\beta} = \sin\beta$, with $\beta_z = -\lambda - \pi/2 - \omega t$ and $\beta_x = \phi - \pi/2$. The meaning of these parameters are: $\omega = 360/24 = 15[^\circ/h]$ is the angular rotation speed of the earth, t is the time elapsed from when the ECI and ECEF frames were aligned, ϕ is the latitude and λ the longitude of the place on the earth. See the appendix for details.

| Horizontal | ECI | ECEF |
|--|---|--|
| Elevation (a) [$-90^\circ, 90^\circ$] | Declination (δ) [$-90^\circ, 90^\circ$] | Declination (δ) [$-90^\circ, 90^\circ$] |
| Azimuth (A) [0, 24]h clockwise+ | right ascension (α) [0,24h] clockwise- from γ | hour angle (h) clockwise+ [0, 24h] from south meridian |

Table I: Position angles in definitions in different reference frames.

IV. ENERGY PRODUCED BY SOLAR PANELS

A. Panel orientation

The orientation of the panel is assigned via the normal to the surface of the panel \mathbf{n} , which is specified through a pair of angles: the altitude a - also called elevation or tilt angle, and the Azimuth (A). Elevation is measured from the horizon along the vertical, while the azimuth is positive clockwise. Instead of the altitude it may be sometimes convenient to specify the zenith angle $\xi = 90 - a$.

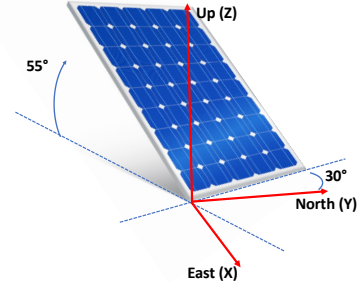


Figure 4: Example of panel orientated towards west ($A = 330^\circ$) and tilted of $a = 55^\circ$ (Creative Commons, authors unknown).

For example, a panel oriented towards west of 30° and tilt angle $a = 55^\circ$ is specified as $A = -30^\circ, a = 55^\circ$ (see Figure). Clearly, the Cartesian coordinates of the normal are $\mathbf{n} = (\cos\xi, \sin\xi\cos A, \sin\xi\sin A)$.

The global solar irradiance (energy per unit time and per unit area) hitting the surface of the PV panel is the sum of three contributions: direct beam, diffuse and reflected irradiance [10]. The amount of these contributions depend on three main elements: (i) panel orientation, (ii) path of the sun in the sky, (iii) weather condition. To keep the analysis simple and since we want to characterise the difference among nearby solar panels, we will focus only on the first contribution due to direct beam irradiation in clear days.

The value of solar irradiation at the mean distance of the earth from the sun on a surface normal to the sun is called the solar constant G_{sc} , and its current estimation is $G_{sc} = 1360W/m^2$. The maximum value of the direct irradiation is approximately $1000 W/m^2$ at sea level on a clear day. With the current technologies is about 10% to $\approx 23\%$ of the solar energy is converted into electrical energy by a solar panel. We will then assume that the maximum power generated by our panels is $G_0 = 100W/m^2$.

B. Energy production

The power produced at a given time by a unit square surface can be computed as:

$$G_f = G_0\cos\Theta = G_0(\mathbf{d} \cdot \mathbf{n})$$

where Θ is the angle between the position of the sun in the sky (and hence the direction of incidence ray on the surface of the PV panel) \mathbf{d} , and the normal to the surface of the panel \mathbf{n} . The energy that recharges the battery during an infinitesimal time interval dt is:

$$dE_C(t) = \begin{cases} G_f dt & b(t) < B \\ 0 & b(t) = B \end{cases}$$

where $b(t)$ is the battery level at time t and B the battery capacity. The infinitesimal energy discharged from the battery is:

$$dE_D(t) = \begin{cases} P(t) dt & b(t) > 0 \\ 0 & b(t) = 0 \end{cases}$$

where $P(t)$ is the power required by the attached operating edge node. The energy stored in the battery at time t is:

$$b(t) = \int dE_C(t) - dE_D(t) \quad (2)$$

The amount of energy produced over a period t_0, t_1 by the panel that cannot be stored nor used is called the *energy loss*, E_L . This quantity can be computed as difference of the energy entering the battery of infinity capacity and into a battery of finite capacity is:

$$E_L = \int_{t_0}^{t_1} G_f(t) dt - \int_{t_0}^{t_1} P(t) dt - \int_{t_0}^{t_1} dE_C(t) \quad (3)$$

V. BASELINE RESULTS

| | | |
|------------------------------|----------|---------------|
| Idle power consumption | P_I | 2.5 W |
| Working power consumption | P_W | 7.0 W |
| Power required to send tasks | P_S | 0.5 W |
| PV power generation | P | 25 W, 35W |
| Battery capacity | B | 80 Wh, 120 Wh |
| Time interval with no sun | T_{NS} | |

Table II: Parameters definition and value ranges

We report here some general result useful to motivate the proposal. The main parameters and their range are reported in table II.

A. Charge-discharging cycles

The energy accumulated in a battery of single edge station follows a charging discharging cycle that depends on the generated/consumed energy and the battery capacity. A well-defined system should be able to fully charge the battery in a sunny day and supply the device at its maximum computation speed starting from a fully charged battery, i.e. $B \geq E > P_W \times T_{NS}$. Figure 5 shows $b(t)$ from Equation 2 for two days.

1) *Effect of PV orientation*: Figure 6 shows how the tilt angle that produces the maximum power depends on the day. Rotation from south (azimuth=180) towards west (azimuth=200) shifts the time when the maximum power is generated and pushes production more towards the sunset time.

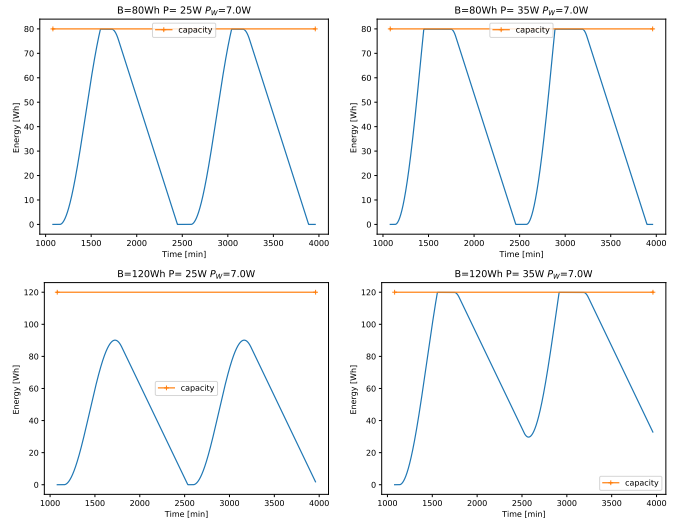


Figure 5: Example charge-discharge cycles over two days. Poor design due to insufficient battery (upper figures); insufficient PV performance (bottom left). The bottom rightmost figures shows a correct design that provides good behaviour.

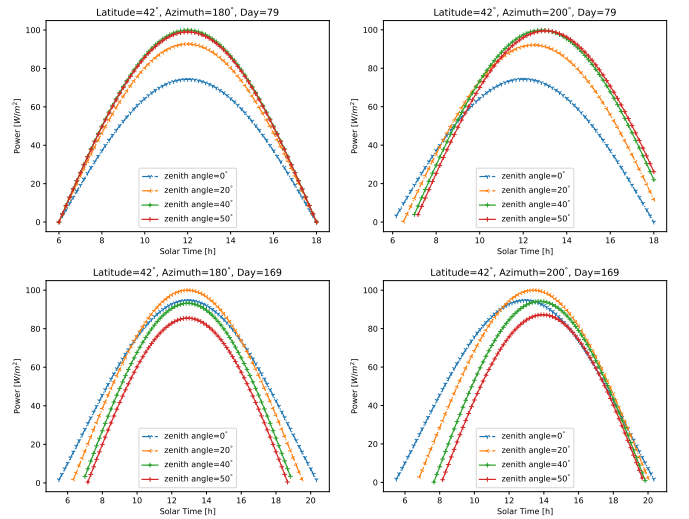


Figure 6: Example of power generated during the equinox (day 79), and summer solstice (day 169), for different elevation angles.

VI. SEEKER-GIVER: AN ALGORITHM FOR GREEN COOPERATION.

The idea of the algorithm is based on the observation that since the system is not connected to a grid when a battery is fully charged, further energy coming from the PV is not utilised (green *energy loss*). The proposed algorithm assumes a set of edge nodes connected in a full mesh via a wireless communication channel. The algorithm divides the operating period of nodes into time slots of equal length, say of some minutes indexed as $k = 0, 1, \dots$. Let e_i^k be the accumulated energy at the end of time slot k , expressed as percentage of the capacity B . If the accumulated energy at node i is higher than

a threshold value, say $e_i^k \geq T_1$ the node announces itself as a surplus or energy *giver* node, while the node whose energy is $e_n^k \leq T_2$ is called an energy *seeker* node. The nodes form two sets, named the Giver set GS and the Seeker Set ES . To match the giver with a seeker, nodes in the two sets are sorted according to their battery level to form two lists, ES' and EG' . The first node in order list ES' is the one with the lowest stored energy, while the first in GS' has the highest accumulated value. Ties are broken based on ids. The value $n = \min\{|ES|, |GS|\}$ is computed. Then the first node in the ES' set is matched with the first node in the GS' set, the second one with the second, etc. until n pairs are determined.

A. Results

We now present some preliminary numerical results of the above algorithm. Results are obtained numerically with time steps of 1 min at equinox day, sunny clear day, latitude $\phi = 42^\circ$.

Experiment 1

This experiment considers two nodes with same orientation, $A = 180^\circ$ and $\xi = 42^\circ$. Figure 7 shows the charge-discharge cycle among an energy giver and energy seeker node over a four days. In this experiment, node 1 requires full power P_W for all days and eventually becomes seeker, while the other node (node 0) is in idle state and is a giver. The top graph shows how node 0 is subject to energy loss events, while node 1 basically discharges the whole battery. This mean in our off-grid assumption that node 1 needs to move into a frozen state and rebooted when energy is available again. The bottom graph shows the cycles for $T_1 = 0.5$ and $T_2 = 0.2$. Task offloading costs $0.5W$, i.e., when offloading the sender node (seeker) consumes $P_I + P_S$ while the giver node $P_W + P_S$. We can see how node 1 never runs out of energy. The difference in the slope of the energy demarcates the time when offloading occurs.

Experiment 2

In the second experiment we considered four edge nodes with the following orientations: $\xi_1 = 20^\circ, A_1 = 120^\circ, \xi_2 = 35^\circ, A_2 = 120^\circ, \xi_3 = 35^\circ, A_3 = 130^\circ, \xi_4 = 42^\circ, A_4 = 180^\circ$. A trace over four days is reported in Figure 8. The first two nodes are idle all the days, while the other are working. Again, the cooperation shows how the working nodes never goes out of energy. The energy loss without cooperation was evaluated from Equation 3 to $E_L = 787.5Wh$, while under cooperation it was $E_L = 747.31Wh$. This reduction is due to offloading.

VII. CONCLUSION

In this paper we have studied a deploy configuration of edge nodes supplied by PV panels. Using numerical models we provide a first assessment of the advantage of performing cooperation among edge nodes with the goal of maximising the use of solar energy. The algorithm is a first step towards a new class of energy-aware resource sharing and cooperation among nodes.

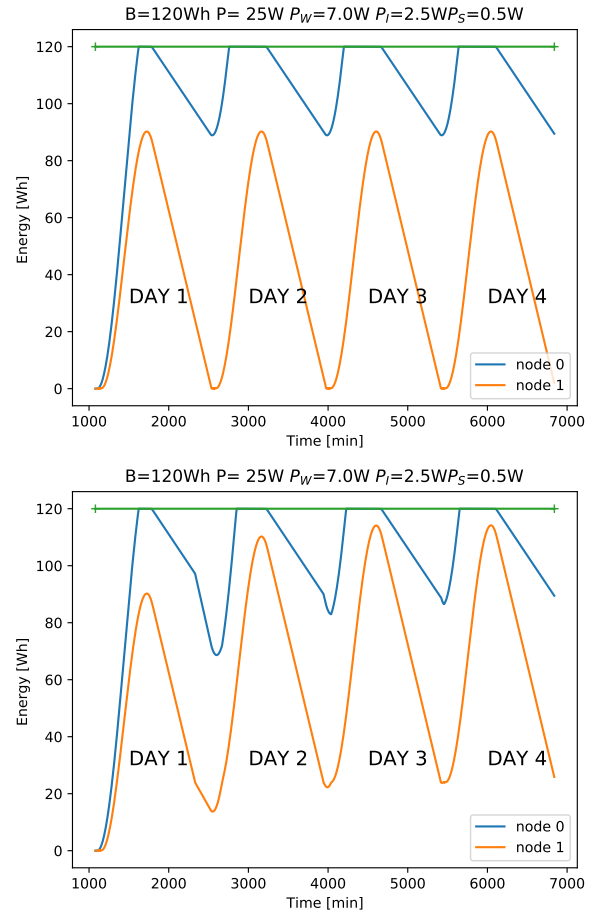


Figure 7: Example of algorithm with $T_1 = 0.5$ and $T_2 = 0.2$. No cooperation (top figure), with cooperation (bottom)

APPENDIX

Consider two right-handed Cartesian reference frames $F = \{\mathbf{e}_1 \mathbf{e}_2 \mathbf{e}_3\}$ and $F' = \{\mathbf{e}'_1 \mathbf{e}'_2 \mathbf{e}'_3\}$ with the same origin, and let $\mathbf{p} = (x_1, x_2, x_3)$ be the coordinates of a point in frame F . The coordinates of the same point in F' are related to the coordinated of F through a linear mapping, defined by a change-of-basis matrix $\mathbf{R}_F^{F'}$, $\mathbf{p}' = \mathbf{R}_F^{F'} \mathbf{p}$. From the equality:

$$\begin{aligned} \mathbf{p} &= \sum_i \mathbf{e}_i x_i = \sum_i \left(\sum_j \mathbf{e}'_j x'_{ji} \right) x_i = \sum_i \sum_j \mathbf{e}'_j x'_{ji} x_i \\ &= \sum_j \mathbf{e}'_j \left(\sum_i x'_{ji} x_i \right) \end{aligned}$$

where x'_{ji} is the j -th coordinates of \mathbf{e}_i in F' , we get:

$$\mathbf{R}_F^{F'} = \begin{pmatrix} x'_{11} & x'_{12} & x'_{13} \\ x'_{21} & x'_{22} & x'_{23} \\ x'_{31} & x'_{32} & x'_{33} \end{pmatrix}$$

The i -th column vector:

$$\mathbf{c}_i = \begin{pmatrix} x'_{1i} \\ x'_{2i} \\ x'_{3i} \end{pmatrix}$$

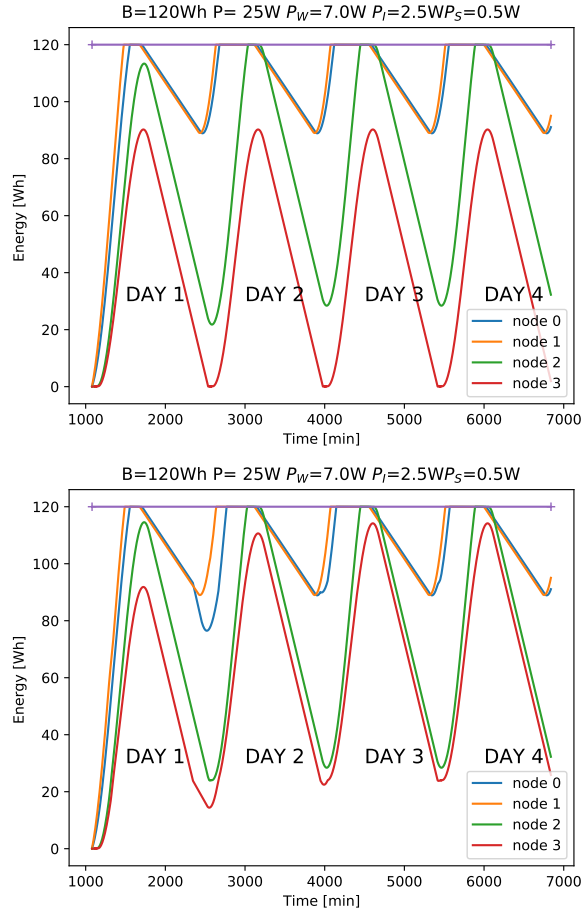


Figure 8: Example of algorithm with four nodes having slightly different PV orientation, with $T_1 = 0.5$ and $T_2 = 0.2$. No cooperation (top), with cooperation (bottom).

is the coordinates of \mathbf{e}_i in F' . To find the coordinate of \mathbf{p} in another frame F'' , one can similarly find a matrix $\mathbf{R}_{F'}^{F''}$ where the i -th column is the coordinate of \mathbf{e}_i' in F'' . We have:

$$\mathbf{p}'' = \mathbf{R}_{F'}^{F''} \mathbf{p}' = \mathbf{R}_{F'}^{F''} \mathbf{R}_F^{F'} \mathbf{p}$$

so that

$$\mathbf{R}_{F'}^{F''} = \mathbf{R}_{F'}^{F''} \mathbf{R}_F^{F'}$$

Of particular interest, are the coordinate changes due to a rotation of around an axis. Assume counterclockwise rotations as positive (CCW+) around an axis of F . The change-of-basis matrix that encodes a clockwise rotation of an angle β around x_i , is:

$$R_{x_1}(\beta) = \begin{pmatrix} 1 & 0 & 0 \\ 0 & c_\beta & -s_\beta \\ 0 & s_\beta & c_\beta \end{pmatrix}$$

$$R_{x_3}(\beta) = \begin{pmatrix} c_\beta & -s_\beta & 0 \\ s_\beta & c_\beta & 0 \\ 0 & 0 & 1 \end{pmatrix}$$

where $c_\beta = \cos(\beta)$, $s_\beta = \sin(\beta)$, where β is the angle on the axis \mathbf{e}_i between F and F' . The change-of-base matrix

is the products of matrixes required to rotate F' until it is superimposed to F .

A. Transformation from ECI to ECEF

The relationship between the ECEF and the ECI frame is a counterclockwise rotation of ωt around the x_3 axis, where t is the time elapsed from when the two frames were aligned and $\omega = 360/24 = 15[^\circ/h]$:

$$R_z(-\omega t)$$

B. Transformation from ECEF to NEU

To align a NEU frame at latitude ϕ and longitude λ to the ECEF, the NEU frame has to rotate clockwise of $\pi/2 + \lambda$ around x_3 , to align the up-axis with the Z_{ECEF} -axis and counterclockwise of $\phi - \pi/2$ around the x_1 , to align the east-axis with the X_{ECEF} -axis. Hence:

$$R_{ECEF}^{NEU}(\phi, \lambda) = R_{x_1}(\phi - \pi/2) R_{x_3}(-\lambda - \pi/2)$$

C. Sun movements and position

The position \mathbf{d} of the sun in the sky as seen by an observer at latitude ϕ and longitude λ at time t is then:

$$\mathbf{d} = R_{ECEF}^{NEU}(\phi, \lambda) \mathbf{d}_{ECI}$$

which is Equation 1.

REFERENCES

- [1] <https://www.statista.com/>.
- [2] M. Iorga, L. Feldman, R. Barton, M. J. Martin, N. S. Goren, and C. Mahmoudi, "fog computing conceptual model," NIST, Tech. Rep., 2018.
- [3] H. Feng, G. Mu, S. Zhong, P. Zhang, and T. Yuan, "Benchmark analysis of yolo performance on edge intelligence devices," *Cryptography*, vol. 6, no. 2, 2022.
- [4] L. Lannelongue, J. Grealey, and M. Inouye, "Green algorithms: Quantifying the carbon footprint of computation," *Advanced Science*, vol. 8, no. 12, p. 2100707, 2021.
- [5] A. Gougeon, B. Camus, and A.-C. Orgerie, "Optimizing green energy consumption of fog computing architectures," in *2020 IEEE 32nd International Symposium on Computer Architecture and High Performance Computing (SBAC-PAD)*, 2020, pp. 75–82.
- [6] J. Wan, B. Chen, S. Wang, M. Xia, D. Li, and C. Liu, "Fog computing for energy-aware load balancing and scheduling in smart factory," *IEEE Transactions on Industrial Informatics*, vol. 14, no. 10, pp. 4548–4556, 2018.
- [7] A. Hazra, M. Adhikari, T. Amgoth, and S. N. Srirama, "Fog computing for energy-efficient data offloading of iot applications in industrial sensor networks," *IEEE Sensors Journal*, vol. 22, no. 9, pp. 8663–8671, 2022.
- [8] M. Adhikari and H. Gianey, "Energy efficient offloading strategy in fog-cloud environment for iot applications," *Internet of Things*, vol. 6, p. 100053, 2019. [Online]. Available: <https://www.sciencedirect.com/science/article/pii/S2542660519300265>
- [9] P. Cooper, "The absorption of radiation in solar stills," *Solar Energy*, vol. 12, no. 3, pp. 333–346, 1969. [Online]. Available: <https://www.sciencedirect.com/science/article/pii/0038092X69900474>
- [10] S. A. Kalogirou, *Solar energy engineering : processes and systems*. Elsevier/Academic Press, 2014.